Study of water impact and entry of a free falling wedge using CFD simulations

Arun Kamath*, Hans Bihs, Øivind A. Arntsen

Department of Civil and Environmental Engineering, Norwegian University of Science and Technology (NTNU), 7491 Trondheim, Norway

Journal of Offshore Mechanics and Arctic Engineering, 2017, **129** 3, pp. 031802-031802-6.
DOI: http://dx.doi.org/10.1002/gghh.pppll20122

Abstract

Many offshore constructions and operations involve water impact problems such as water slamming onto a structure or free fall of objects with subsequent water entry and emergence. Wave slamming on semi-submersibles, vertical members of jacket structures, crane operation of a diving bell and dropping of free fall lifeboats are some notable examples. The slamming and water entry problems lead to large instantaneous impact pressures on the structure, accompanied with complex free surface deformations. These need to be studied in detail in order to obtain a better understanding of the fluid physics involved and develop safe and economical design. Numerical modelling of a free falling body into water involves several complex hydrodynamic features after its free-fall such as water entry, submergence into water and resurfacing. The water entry and submergence lead to formation of water jets and air cavities in the water resulting in large impact forces on the object. In order to evaluate the forces and hydrodynamics involved, the numerical model should be able to account for the complex free surface features and the instantaneous pressure changes. The water entry of a free-falling wedge into water is studied in this paper using the open source CFD model REEF3D. The vertical velocity of the wedge during the process of free fall and water impact are calculated for different cases and the free surface deformations are captured in detail. Numerical results are compared with experimental data and a good agreement is seen.

1 Introduction

Water impact and water entry are significant problems in the field of offshore engineering. Various engineering problems during operations with offshore constructions such as wave slamming on jacket structures and semi-submersibles are water slamming problems. In the case of free-falling bodies such as free-fall life boats used for quick evacuation of personnel from offshore platforms and vessels, water impact, water entry and emergence are of significance to the safety and stability of the lifeboat. The hydrodynamics associated with water slamming,

*Corresponding author, arun.kamath@ntnu.no

entry and emergence of the body are complex due to the large instantaneous pressure changes and free surface deformations involved in the process. Design guidelines such as the DNV-OS-E406 DNV (2009) call for large amount of rigorous testing for the design of free-fall life boats. This requires a large amount of experiments which can be expensive and time consuming. In this context, numerical modeling of free-falling objects can be carried out to develop competence to simulate free-fall lifeboats and contribute to the knowledge required for their design.

Computational Fluid Dynamics (CFD) provides an opportunity to simulate complex hydrodynamic problems as it solves the Navier-Stokes equations with few assumptions. This provides a very detailed solution of the flow problem. In the case of free-falling objects, the motion of the object, the impact of the object with water, the free surface deformations associated with water impact, water entry and the re-emergence of the object can be modeled in an accurate manner. A CFD model solves the fluid hydrodynamics with few assumptions and can account for the nonlinearities arising from the fluid viscosity and rotational flow. This is important in the case of water impact problems as several authors have reported breaking wave-like features associated with the impact of an object onto water in their experimental studies Greenhow and Lin (1983) Greenhow (1989).

Before complex simulations involving free-fall lifeboats are simulated using a CFD-based model, the numerical model has to be validated using simpler test cases such as the water impact of a wedge. Several authors have studied this problem in current literature using analytical approaches and experimental studies.

The first analytical approaches to calculate water impact problems were proposed by von Karman (1929) and Wagner (1932). They used equivalent plates to identify the water plane area and determine the impact pressure due to the slamming of a body on calm water. The high speed water-entry of a wedge and a horizontal cylinder was studied experimentally by Greenhow and Lin (1983). They proposed that for large motions of the free surface due to the impact of an object on calm water, linear theory cannot be applied to obtain sufficiently accurate results. This would in turn impact the solution for the water-exit phase of the problem. The free surface features associated with the water impact are shown to resemble breaking waves. In the event that the rotational and viscous motions are neglected in this case, the water jets predicted by linear theory are found to be too high resulting in a wrong depiction of the free surface profile. The water-exit of a horizontal cylinder was studied by Greenhow (1989) and observed the formation of large regions of strongly negative pressure around the surface of the cylinder during water-exit. This is found to be the cause of the localised breaking wave-like formations seen during water impact of the cylinder. The water entry and exit problem due to constant velocity impact was experimentally studied by Tveitnes et al. (2008) and presented wetting factors for the wedge and the flow momentum drag coefficients for different deadrise angles of the wedge. They also reported that significant dynamic noises limits the accuracy of the results after the immersion of the wedge.

In terms of CFD modeling of complex free surface features around floating bodies in water, several important works are found in current literature. A framework for modeling ship hydrodynamics using dynamic overset grids was presented by Carrica et al. (2007). A two-phase model for floating bodies was presented by Calderer et al. (2014) using a curvilinear immersed boundary method to treat the solid-fluid boundary. The impact, submergence and emergence of the object in free-fall impact problems involves large velocities during the free fall, large and instantaneous pressure and velocity changes during impact, submergence and

emergence of the object. In order to capture the fluid physics in these challenging cases, the numerical model used for these simulations needs to be computationally efficient and accurate.

In this paper, the impact of a wedge on still water is simulated in two-dimensions using the open-source CFD model REEF3D Alagan Chella et al. (2015). The model has been previously used for calculating breaking wave kinematics Alagan Chella et al. (2015), propagation, shoaling and wave breaking over a submerged bar Kamath et al. (2015*b*) and non-breaking wave forces Kamath et al. (2015*a*). The model is validated for the free-fall wedge problem by comparing the numerical results with experimental data presented by Yettou et al. (2006). The motion of the wedge in the two-dimensional simulations is restricted to the x-z plane and includes only heave and pitch motions. Further, simulations are carried out with different densities of the free-falling wedge. The position of the wedge, the velocity of the wedge and the free surface around the wedge at impact are studied to gain further insight into the water impact problem.

2 Numerical Model

The incompressible Reynolds-Averaged Navier-Stokes (RANS) equations are used to solve the fluid flow problem:

$$\frac{\partial u_i}{\partial x_i} = 0 \tag{1}$$

$$\frac{\partial u_i}{\partial t} + u_j \frac{\partial u_i}{\partial x_j} = -\frac{1}{\rho}\frac{\partial p}{\partial x_i} + \frac{\partial}{\partial x_j}\left[(\nu + \nu_t)\left(\frac{\partial u_i}{\partial x_j} + \frac{\partial u_j}{\partial x_i}\right)\right] + g_i \tag{2}$$

where u is the time averaged velocity, ρ is the density of water, p is the pressure, ν is the kinematic viscosity, ν_t is the eddy viscosity, t is time and g is the acceleration due to gravity. Chorin's projection method Chorin (1968) is used for the pressure treatment and a preconditioned BiCGStab solver van der Vorst (1992) is used to solve for the pressure.

Turbulence modelling is carried out based on Durbin's modification Durbin (2004) of the two equation k-ω model proposed by Wilcox Wilcox (1994). Eddy viscosity, ν_t, is bounded to avoid unphysical overproduction of turbulence in strained flow as shown by DurbinDurbin (2009). The large difference in density of air and water in a two-phase model leads to an overproduction of turbulence at the interface due to large strain. For this reason, free surface turbulence damping is introduced around the interface based on the studies by Naot and Rodi Naot and Rodi (1982).

The fifth-order conservative finite difference Weighted Essentially Non-Oscillatory (WENO) scheme proposed by Jiang et al. Jiang and Shu (1996) is used for the discretization of convective terms for the velocity U_i, the level set function ϕ, turbulent kinetic energy k and the specific turbulent dissipation rate ω. A TVD third order Runge-Kutta explicit time scheme developed by Harten Harten (1983) is employed for time discretization in the model. It is a three-step scheme and involves the calculation of the spatial derivatives three times per time step. This scheme is used for the time advancement of the level set function and the reinitialisation equation.

A Cartesian grid is used in the numerical model for spatial discretization. The Immersed Boundary Method (IBM) Peskin (1972) is used to incorporate the boundary conditions for complex geometries. In the current study, a multiple directional ghost cell IBM (MGCIBM) implemented by Bihs Bihs (2011) using object oriented programming techniques is used, where the ghost cell values can be updated from multiple directions. The ghost cells store

multiple values and return a particular value when called from a particular direction. The free surface is obtained using the level set method where the zero level set of a signed distance function, $\phi(\vec{x}, t)$ is used to represent the interface between air and water. Moving away from the interface, the level set function gives the closest distance of the point from the interface. The sign of the function represents the two fluids across the interface. The level set function is reinitialised after every iteration using a partial differential equation (PDE) based reinitialisation procedure presented by Sussman et al.Sussman et al. (1994) to retain its signed distance property after convection.

A 6 degrees-of-freedom (6DOF) algorithm is implemented to model moving objects. The surface of the object is also described using the level set function. The motion of the wedge is accounted for using the 6DOF equations and the level set function is used to represent the motion of the surface of the moving object. The advantage of using the level set method is that the use of overset meshes or the need to re-mesh after every motion of the object is avoided, resulting in a more computationally efficient simulation. The computational efficiency of the program is increased by using MPI (Message Passing Interface) to run it as a fully parallel code on multiple processors. Here the domain is decomposed into smaller pieces and each assigned to a processor. So the program runs separately on each processor and the values between the processes are communicated using the MPI library.

3 Results

3.1 Grid convergence study

First, a grid convergence study is carried out with a free-falling wedge onto still water of depth $d = 2.0$ m. The wedge has a bottom angle of 25° with respect to the x-axis, a width of 1.2 m. The wedge is allowed to fall freely with the tip of the wedge held 2.5 m above the still water level. An illustration of the wedge used in the study is presented in Fig. (1). The density of the wedge is $\rho_{wedge} = 466.7$ kg/m^3. Simulations are carried out with grid sizes $dx = 0.05$ m, 0.03 m, 0.02 m and 0.01 m. The simulations are carried out for a duration of 12 s. The position and vertical velocity of the wedge during the free-fall are calculated and the comparison of the numerical results for the different grid sizes are presented in Fig. (2a) and (2b) respectively. The numerical results for 5 s of motion are presented in Fig. (2) to focus around the free fall and the moment of water impact of the wedge. It is seen that the numerical results converge to similar values as the grid is refined. The results for $dx = 0.02$ m and 0.01 m are found to be similar for both the position of the wedge and its vertical velocity. From these results for the grid convergence it is concluded that further simulations can be carried out with a grid size of $dx = 0.02$ m. The major difference in the results on improving

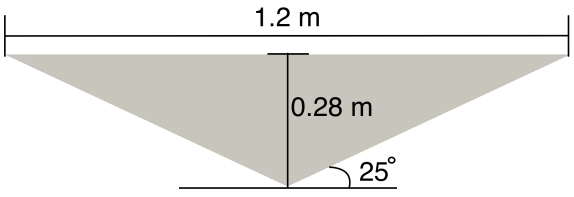

Figure 1: Illustration of the wedge used for free fall wedge simulations in this study

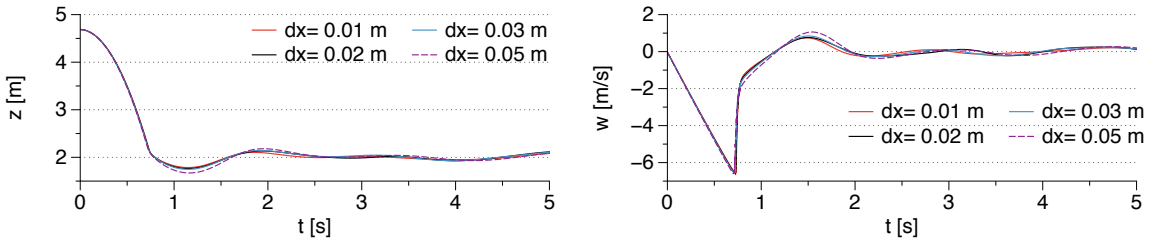

(a) vertical position of the free-falling wedge (b) vertical velocity of the free falling wedge

Figure 2: Grid convergence studies for a free-falling wedge

the grid resolution is the improved representation of the water jet formed on the impact of the wedge. On a coarser grid, owing to poorer pressure and velocity solutions, produces a poorer representation of the water jet formed on impact as seen in Fig. (3).

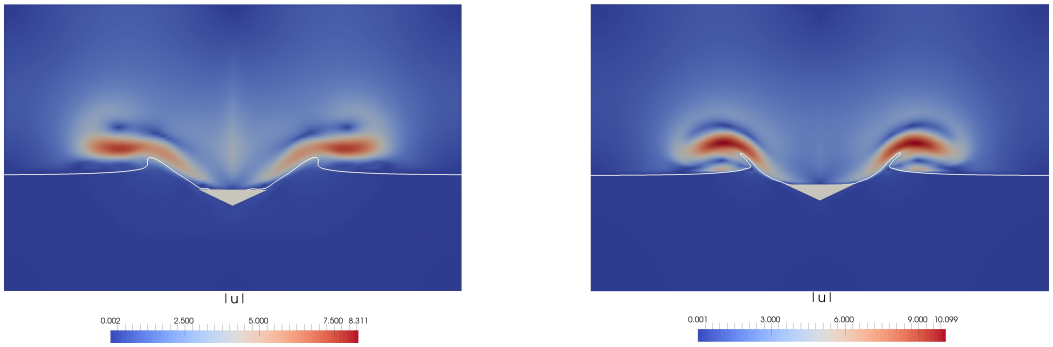

(a) $t = 1.11$ s, $dx = 0.05$ m (b) $t = 1.11$ s, $dx = 0.02$ m

Figure 3: Effect of grid resolution on the free surface features during the impact of the wedge

3.2 Comparison with experimental data

The numerical model is validated by comparing the results for the vertical position and velocity of the free-falling wedge with experimental data from Yettou *et al.* Yettou et al. (2006). The wedge used in the experiments is 1.2 m long, symmetrical about the y-axis with the sides making a 25° angle to the x-axis, with a density of $\rho_{wedge} = 466.7$ kg/m^3 and the tip of the wedge is 1.3 m from the still water level in a tank with a water depth of 1.0 m. The two-dimensional numerical domain is 8.0 m wide and 4.0 m deep with a grid size of $dx = 0.02$ m with a water depth of $d = 1.0$ m and the wedge is placed with its tip 1.3 m from the still water level as in the experiments.

The numerical results for the vertical position and velocity of the free-falling wedge are compared to the experimental data and presented in Fig. (4). The comparison of the position of the wedge during its free fall and after impact with the water with experimental data in Fig. (4a) are well represented in the numerical model. The comparison of the numerical and experimental results for the vertical velocity of the wedge also presents a good agreement in Fig. (4b). These results show that the vertical velocity of the wedge increases linearly during

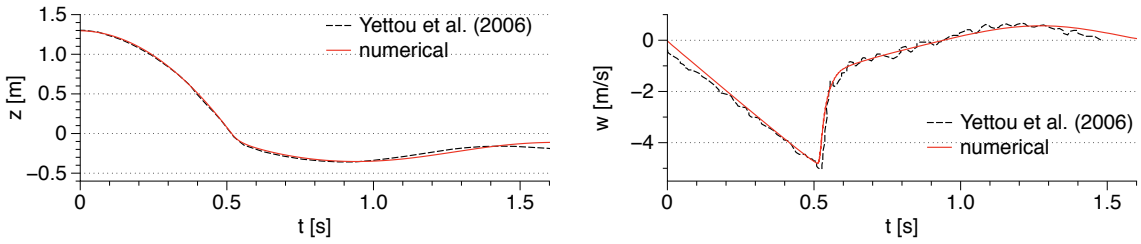

(a) vertical position of the free-falling wedge (b) vertical velocity of the free falling wedge

Figure 4: Comparison to numerical results to experimental data from Yettou et al. (2006)

free fall until impact with the water surface at $t = 0.53$ s. At this moment the position of the wedge in Fig. (4a) has a zero-crossing indicating the wedge has impacted the free surface. At the same time, in Fig. (4b), the vertical velocity of the wedge reaches a maximum and abruptly changes the direction of motion. The wedge in this case is much lighter than water and thus penetrates the water only for a short while after impact. Further, it floats on the surface of the water and moves about the free surface due to the disturbance caused to the free surface on impact.

3.3 Free-falling wedges of different densities

Further the impact of a free-falling wedge on still water is studied for different densities of the wedge. The simulations are carried out in a two-dimensional tank with a width of 8.0 m and a height of 5.0 m with a water depth of 2.0 m with a grid size of $dx = 0.02$ m. The wedge is 1.2 m wide and symmetrical making an angle of 25° with the x-axis with the tip of the wedge 2.78 m above the still water level. Wedge densities ρ_{wedge} of 466.7, 600.0, 800.0 and 900.0 kg/m^3 are considered. The results for the position and the vertical velocity of the free-falling wedge for the different densities of the wedges are presented in Fig. (5). It is seen from

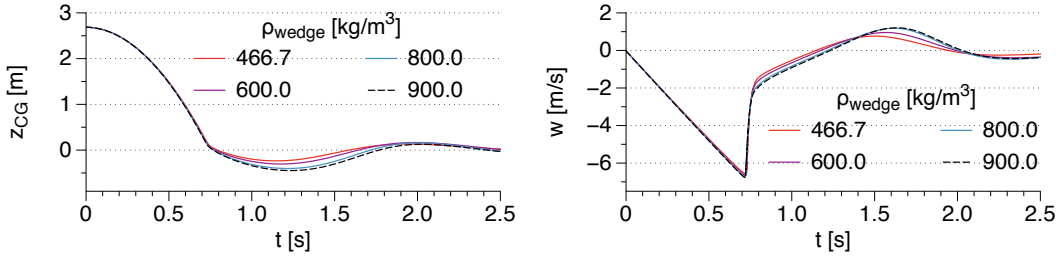

(a) vertical position of the free-falling wedge (b) vertical velocity of the free falling wedge

Figure 5: Numerical results for vertical position and velocity of the free-falling wedge for different densities of the wedge

Fig. (5a) that the wedge with the highest density $\rho_{wedge} = 900.0$ kg/m^3 obtains the deepest immersion into water after impact with its lowest position just after impact $z_{min} = -0.45$ m. The depth of immersion of the wedge reduces with reducing density of the wedge with $z_{min} = -0.40$ m for $\rho_{wedge} = 800.0$ kg/m^3 and $z_{min} = -0.30$ m and -0.23 m for $\rho_{wedge} =$

600.0 and 466.7 kg/m^3 respectively. Figure (5b) shows that the maximum vertical velocity of impact of w_{max} = -6.77 m/s is calculated for the wedge of the highest density $\rho_{wedge} = 900.0$ kg/m^3. The variation of the depth of immersion of the wedge is found to vary linearly with the density of the free-falling wedge. The position of the wedge plotted in Fig. (5a) also shows that after the wedge re-emerges towards the free surface, minor oscillations about the free surface are seen due to the disturbance caused to the free surface due to the impact. Also, larger oscillations in the position of the wedge are seen between $t = 6 - 8$ s. This is due to the waves generated on impact that reflect from the walls and travelling back towards the wedge. The effect of the reflected waves is also seen in the higher vertical velocities of the floating wedge in Fig. (5b).

The process of free-fall and water impact for the wedge with density $\rho_{density} = 600.0$ kg/m^3, is presented in Fig. (6). The wedge is at its initial position in Fig. (6a) at $t = 0.0$ s, with its tip 2.5 m above the still water level in a tank with a water depth of 2.0 m. The wedge is allowed to fall freely and the wedge approaches the water free surface and the tip of the wedge just makes contact with the still water surface in Fig. (6b) at $t = 0.72$ s and the process of water impact begins here. The large velocities in the air indicate the high velocity with which the wedge approaches the water. The wedge penetrates the free water surface at $t = 0.74$ s in Fig. (6c) and the water begins to rise along the side surfaces of the wedge in a symmetrical fashion. In Fig. (6d), the wedge has further penetrated the water and the top of the wedge is almost along the raised free surface around the wedge at $t = 0.77$ s. As the wedge further enters the body of water, the displaced water rising along the edges of the wedge shoots above the still water level in Fig. (6e). The shape of this jet of water is similar to that of an overturning wave crest. This water jet is further developed in Fig. (6f) as the wedge penetrates further into the water at $t = 0.90$ s. A cavity is formed behind the wedge as it pushes the water free surface downward and outward along its edges. In Fig. (6g) the wedge is at its maximum depth of penetration into the water at $t = 1.20$ s and the water jet is fully developed. The re-emergence of the wedge to the free surface at $t = 1.89$ s is seen in Fig. (6h). The elevated free surface under the wedge is seen to be elevated as the water in the surroundings rushes to fill in the cavity formed about the free surface due to the entry and impact of the wedge. Since the density of the wedge is lower than the density of the water, the wedge does not submerge into the water mass. Thus, the water free surface does not close the cavity formed behind the wedge and the wedge floats back to the free surface. Further oscillations of the wedge are caused due to the waves generated by the impact of the wedge hitting the walls on the boundary of the domain and travelling back towards the wedge.

The free surface around the wedge during its impact into water and the developed jets at the point of its maximum penetration is presented for two cases, $\rho_{wedge} = 900.0$ kg/m^3 and 466.7 kg/m^3 in Fig. (7). The wedge penetrates a maximum depth of $z = -0.45$ m at $t = 1.21$ s for $\rho_{wedge} = 900.0$ kg/m^3 according to Fig. (4a) and for $\rho_{wedge} = 466.7$ kg/m^3 it is $z = -0.23$ m at $t = 1.13$ s. The wedge with the higher density impacts the water with a higher momentum and penetrates deeper into the water in the tank compared to the wedge with the lower density. Figure (7a) shows that the water jet developed at the moment of maximum penetration for the denser wedge is longer and cavity formed behind the wedge has steeper slopes compared to those formed for the wedge with lower density in Fig. (7b). The velocity magnitude contours in Figs. (7a) and (7b) show that the motion is more laminar in the case of the wedge with lower density due to the lower momentum of impact. The free surface features and the velocity magnitude contours are symmetrical in both cases.

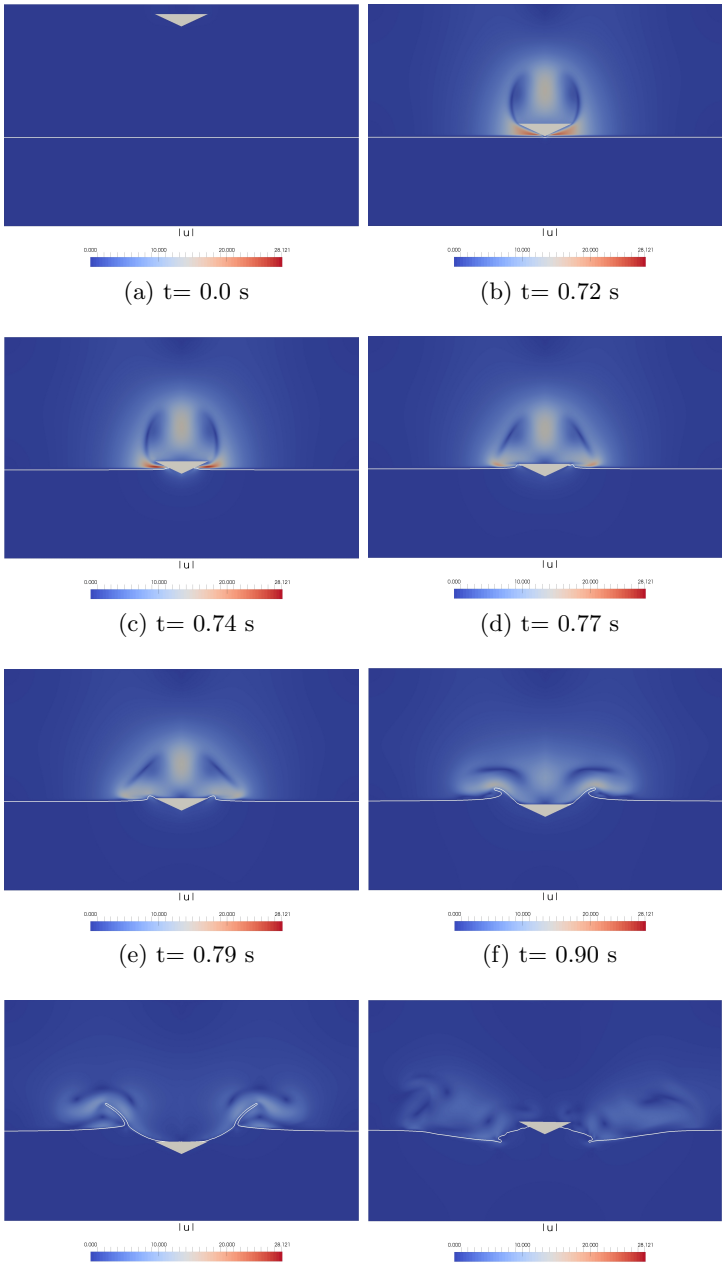

(a) t= 0.0 s (b) t= 0.72 s

(c) t= 0.74 s (d) t= 0.77 s

(e) t= 0.79 s (f) t= 0.90 s

(g) t= 1.20 s (h) t= 1.89 s

Figure 6: Simulation of free-fall of the wedge with $\rho_{wedge} = 600.0$ kg/m^3 and water impact with velocity magnitude contours

The simulation is also carried out in 3D to obtain a three-dimensional view of the slamming and water entry problem for the wedge of density $\rho_{wedge} = 466.7$ kg/m^3. The impact of the the wedge on to the still free surface is shown in Fig.(8) along with the velocity magnitude contours in water. The velocity of the wedge and the position were seen to be similar to the results obtained from the 2D simulations.

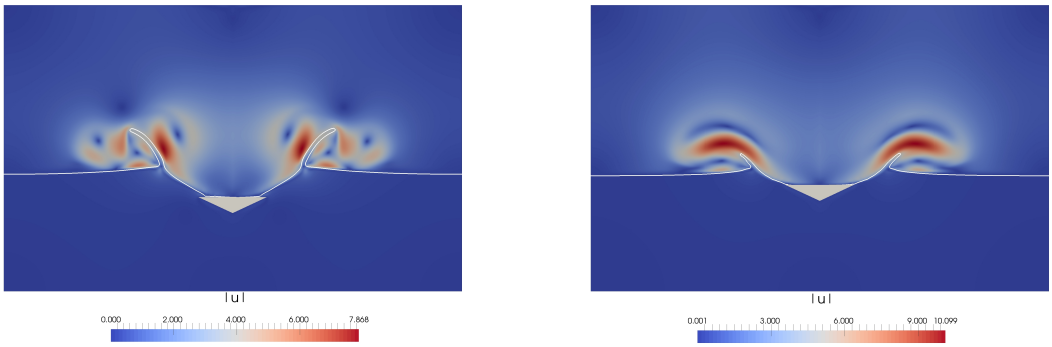

(a) $t = 1.21$ s for $\rho_{wedge} = 900.0$ kg/m^3 (b) $t = 1.13$ s for $\rho_{wedge} = 466.7$ kg/m^3

Figure 7: Free surface around the wedge during maximum penetration into water for the wedges with the maximum and minimum density in this study with velocity magnitude contours

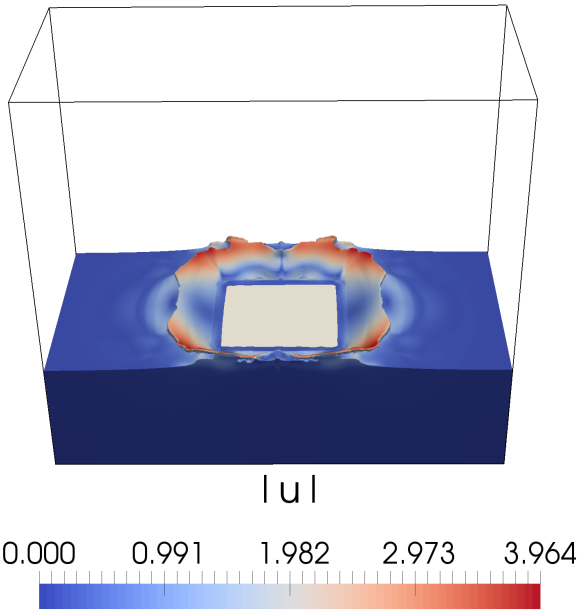

Figure 8: 3D simulation of freely falling wedge impacting still water

4 Conclusions

The open-source CFD model REEF3D is used in this study to evaluate the water impact problem of a symmetrical wedge. The numerical results are compared with experimental data for the vertical position and the vertical velocity of the wedge. A good agreement is seen between the numerical and the experimental results. The rise-up of the water along the edges of the wedge and the formation of the water jet du to the penetration of the wedge into the water mass are well represented by the numerical model.

Simulations are further carried out to study the water impact due to different densities of

the free-falling wedges and the positions and vertical velocity of the wedges in the different cases are studied. The depth of immersion of the wedge tip is found to be directly related to the density of the wedge for a given drop height. The wedge with higher density carries a higher momentum as it impacts the free water surface compared to a lower density wedge. This resulted in different features of the water jet formed on water entry of the wedge. A 3D simulation was also carried out using the model.

The capability of the CFD model to simulate the impact of a freely falling wedge with water and parameters such as the position and the vertical velocity of the wedge along with the free surface features associated with water impact are presented in this study. Further studies are to be carried out to study the effect of the drop height, the pressure and forces acting on the wedge. The knowledge gained from these studies can then be extended to study realistic engineering problems such as the free-fall life boat and contribute to the design process of such systems. The use of CFD simulations to study such problems can greatly help in the development of safe and reliable designs while rigorously testing the system according to the guidelines set by the standards.

Acknowledgements

This research was supported in part with computational resources at NTNU provided by The Norwegian Metacenter for Computational Sciences (NOTUR), http://www.notur.no.

References

Alagan Chella, M., Bihs, H., Myrhaug, D. and Muskulus, M. (2015). Breaking characteristics and geometric properties of spilling breakers over slopes. *Coastal Engineering*, **95**, 4–19.

Bihs, H. (2011). Three-dimensional numerical modeling of local scouring in open channel flow. PhD thesis No. 127, Department of Hydraulic and Environmental Engineering, Norwegian University of Science and Technology, Trondheim, Norway.

Calderer, A., Kang, S. and Sotiropoulos, F. (2014). Level set immersed boundary method for coupled simulation of air/water interaction with complex floating structures. *Journal of Computational Physics*, **277**, 201–227.

Carrica, P.M., Wilson, R.V., Noack, R.W. and Stern, F. (2007). Ship motions using single-phase level set with dynamic overset grids. *Computers and fluids*, **36**(9), 1415–1433.

Chorin, A. (1968). Numerical solution of the Navier-Stokes equations. *Mathematics of Computation*, **22**, 745–762.

DNV (2009). Offshore standard DNV-OS-E406. Det Norske Veritas (DNV), Norway.

Durbin, P.A. (2004). Turbulence closure models for computational fluid dynamics.

Durbin, P.A. (2009). Limiters and wall treatments in applied turbulence modeling. *Fluid Dynamics Research*, **41**, 1–18.

Greenhow, M. (1989). Water-entry and -exit of a horizontal circular cylinder. *Applied Ocean Research*, **10**(4), 191–198.

Greenhow, M. and Lin, W.M. (1983). Massachusetts Institute of Technology, USA.

Harten, A. (1983). High resolution schemes for hyperbolic conservation laws. *Journal of Computational Physics*, **49**, 357–393.

Jiang, G.S. and Shu, C.W. (1996). Efficient implementation of weighted ENO schemes. *Journal of Computational Physics*, **126**, 202–228.

Kamath, A., Alagan Chella, M., Bihs, H. and Arntsen, Ø.A. (2015*a*). Cfd investigations of wave interaction with a pair of large tandem cylinders. *Ocean Engineering*, **108**, 738–748.

Kamath, A., Alagan Chella, M., Bihs, H. and Arntsen, Ø.A. (2015*b*). CFD simulations of wave propagation and shoaling over a submerged bar. *Aquatic Procedia*, **4**, 308–316.

Naot, D. and Rodi, W. (1982). Calculation of secondary currents in channel flow. *Journal of the Hydraulic Division, ASCE*, **108**(8), 948–968.

Peskin, C.S. (1972). Flow patterns around the heart valves. *Journal of Computational Physics*, **10**, 252–271.

Sussman, M., Smereka, P. and Osher, S. (1994). A level set approach for computing solutions to incompressible two-phase flow. *Journal of Computational Physics*, **114**, 146–159.

Tveitnes, T., Fairlie-Clarke, A.C. and Varyani, K. (2008). An experimental investigation into the constant velocity water entry of wedge-shaped sections. *Ocean Engineering*, **35**(14), 1463–1478.

van der Vorst, H. (1992). BiCGStab: A fast and smoothly converging variant of Bi-CG for the solution of nonsymmetric linear systems. *SIAM Journal on Scientific and Statistical Computing*, **13**, 631–644.

von Karman, T. (1929). The impact on seaplane floats during landing.

Wagner, H. (1932). Uber stoss-und gleitvorgange an der oberflache von flussigkeiten.

Wilcox, D.C. (1994). *Turbulence modeling for CFD*. DCW Industries Inc., La Canada, California.

Yettou, E.M., Desrochers, A. and Champoux, Y. (2006). Experimental study on the water impact of a symmetrical wedge. *Fluid Dynamics Research*, **38**, 47–66.